An Adaptive Approach to Topographic Feature Extraction from Digital Terrain Models

Yonghak Song and Jie Shan

Abstract

This study presents an adaptive solution to topographic feature extraction from digital terrain model. First, a slope map is produced by the proposed slope estimator that combines the well-known D8 and finite difference methods. In the second step, the Laplacian of Gaussian (LOG) operator with multiple thresholds is applied to the resultant slope map to determine edge pixels that have local maximum curvature and maximum connectivity. The third step adopts the original and robust marching square algorithms to trace the topographic features. Modification is made to selectively introduce shoulder points according to the local topographic complexity. In comparison to the existing algorithms, the performance of the proposed adaptive marching square algorithm is evaluated in terms of precision and resolution of the extracted features. Digital terrain models over three locations in Antarctica are used for this study. It is shown overall reducing 75 percent of the shoulder points from the robust algorithm will cause 24 percent precision drop in the adaptive method.

Introduction

Recent advances in geospatial data collection technology enable rapid, accurate, and effective acquisition of geographic information. Much of such information is taken the form of digital terrain model (DTM) at its early stage, which needs further processing for a variety of reasons. First, DTM is a regular representation of the reality at a constant resolution not adaptive to the complexity of the real world. The data format may be either too dense for simple terrain or too sparse for complex terrain. Secondly, such data format is not "intelligent," i.e., they do not directly support geospatial query and analysis. Finding interesting objects or features in DTM is not possible without semantically encoding the DTM. DTM can also not be directly used for object-based geospatial analysis such as dimension calculation and buffering. Finally, comparing with object-based or vector data, the volume of DTM is often overwhelming so that certain simplification and abstraction towards the imbedded objects are needed.

Determining interest geospatial objects from DTM is called feature extraction in general. Topographical features can be understood as distinct structure elements, such as a summit or pothole, or in linear form such as a valley or ridge. Cliffs, ditches, pit, dams may also be regarded as topographic features, depending on the fields of applications (Moore *et al.*, 1991). According to Florinsky (1998), interest topographic features can be determined with DTM by using either primary or compound topographic attributes. Primary attributes are specific geometric properties of the topographic surface calculated directly from DTM, such as slope, aspect, and curvature. Compound attributes are estimates of the spatial distribution of specific, biologically significant physical environmental parameters in the landscape, such as incoming solar radiation, soil wetness, watershed, quarry, and drainage network.

Considerable studies have been done on extracting topographic features from DTM. Early work included Mark (1984) and O'Callaghan and Mark (1984) for drainage network extraction, Band (1986) for watershed derivation, Jenson and Domingue (1988) for topographic structure elements, and Tarboton (1997) for flow direction and upslope areas. Miliaresis and Argialas (1999) applied a region-growing segmentation algorithm to find basin and mountain region with predefined thresholds. Being aware of the difficulty of topographic feature extraction solely from DTM, especially in flat regions, rivers, and lake network maps (Turcotte *et al.*, 2001), environmental characteristics (Vogt *et al.*, 2003), and satellite images (Argialas and Tzotsos, 2006) were also used to assist this process. The same study was recently extended to DTM collected from light detection and ranging (lidar) technology for breakline detection (Brügelmann, 2000; Briese, 2004; Brzank *et al.*, 2005), fiducial surface modeling in coastal area (Brock *et al.*, 2001), river corridor topography (Cobby *et al.*, 2001; Bowen and Waltermire, 2002), coastal elevation changes (Woolard and Colby, 2002), and local desert topography transformation due to vegetation transitions (Rango *et al.*, 2000). Moreover, high-resolution Interferometric Synthetic Aperture Radar (IFSAR) DTM was also used by Hooper *et al.* (2003) to determine fault scarps, and by Guthrie and Simental (2003) to derive topographic features. It is noticed that most such studies involve much domain-specific knowledge and hence may not be directly useful for applications different than they originally intended for. As a matter of fact, many topographic features, regardless their domain-specific background, have common characteristics, and their extraction methods should therefore share certain common basis and properties. Based on this consideration, our interest concentrates on one type of generic topographic features whose boundary can be defined based on slope as one primary topographic attribute.

This paper will present an adaptive approach to topographic feature extraction from DTM. The topographic features to be extracted can be segmented into regions whose

School of Civil Engineering, Purdue University, 550 Stadium Mall Drive, West Lafayette, IN-47907 (jshan@ecn.purdue.edu).

Photogrammetric Engineering & Remote Sensing
Vol. 75, No. 3, March 2009, pp. 281–290.

0099-1112/09/7503–0281/$3.00/0

boundary is an equal-slope contour and whose interior is above a certain slope threshold. Our objectives are to detect and locate these features, trace their boundaries, and represent them to a desired fidelity. Such a process should be implemented in an automated manner and evaluated in terms of performance. The proposed approach is mostly based on the techniques in image processing and computer graphics. In this paper, we will first describe the feature model introduced in this study. The proposed method starts with the calculation of a slope map, for which a modified slope estimator combining the properties of D8 method (O'Callaghan and Mark, 1984), and the finite difference method (Fleming and Hoffer, 1979) is introduced to achieve satisfactory results. The second step determines the slope contour value (threshold) for the feature boundary such that it passes the most number of pixels where local maximum curvatures occur. For this purpose, we first apply the Laplacian of Gaussian (LOG) operator (Marr and Hildreth, 1980) by means of multiple thresholding to the slope map to select the edge pixels that can yield maximum connectivity. The slope that corresponds to as many as possible selected edge pixels will be determined as the threshold for feature boundary. The third step is to trace the feature boundary pixels for efficient representation and storage. Adopted for this purpose is the 2D version marching cube algorithm (Lorensen and Cline, 1987), which was originally developed to find iso-surface from 3D data for volume rendering. Although the robust marching cube (square) algorithm (Lopes and Brodlie, 2003) can achieve sub pixel line segments by adding an auxiliary point (called shoulder point) in each DTM cell (pixel), such shoulder points may not be needed at all places due to the spatial variation of the feature boundary complexity. We propose an adaptive marching square algorithm, which selectively adds a shoulder point at places where complex topography occurs. In this way, the amount of shoulder points can be reduced while the extracted feature boundary retains essentially the same or very similar precision. The proposed approach is tested by using three DTM data sets over Antarctica and evaluated in comparison with both the original and robust marching square algorithms in terms of resolution and precision.

Methodology

The section will first describe the introduced feature models, and then depict the three sequential steps of the proposed approach: slope calculation, boundary determination, and boundary tracing.

Feature Model

A proper description on the feature is necessary for its extraction. In our study, a feature is defined as a region that consists of interior and boundary. The feature boundary has a constant slope whereas the feature interior is above certain slope threshold. As shown in Figure 1,

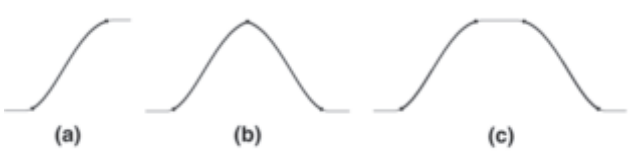

Figure 1. (a) edge and feature; feature with simple edge, and ((b) and (c)) features with compound edges. The dots are the boundary location. The thicker line is interior, the finer line is exterior.

features can be formed by a single edge or a combination of edges in the lateral profile. An edge (thicker line) is bounded by two edge (structure) points (dark dots) that have (local) maximum curvatures (slope change). As pointed out by Morris (1996), a set of points for which one of the principal curvatures has an extremal value can be extracted by the third derivative. They appear as the hinge lines of folds (Ramsay, 1967) and are regarded being significant to a topographic surface (Koenderink, 1990). Thus, we apply the LOG (second derivative) to the slope map (first derivative) derived from the DTM, find the zero-crossings of the LOG as the edge pixels, and connect them as the feature boundary. Figure 2 illustrates the extracted edge lines from a DTM and its slope map in comparison to the extracted edges as a region.

It should be noted that our feature model has some distinctions in comparison with traditional models. It considers not only features formed by a simple edge but by compound edges such as a valley, mount, and plateau (see Figure 1). A feature, in general, is treated as a region with interior and boundary. The feature interior is a collection of pixels whose slopes are over certain threshold, whereas the feature boundary has a constant slope and forms a polygon that can take into account the interior and exterior of a feature.

Slope Calculation

Slope calculation is the first step towards detecting and tracing feature boundaries. Most popular slope calculation methods use a 3×3 neighborhood (Figure 3) around the interest pixel. The D8 method (O'Callaghan and Mark, 1984), also known as the steepest descent, defines the slope as the maximum drop from the central pixel to its eight nearest neighbors. Fleming and Hoffer (1979) proposed the finite difference method that considers the elevation changes in both horizontal and vertical directions. Horn (1981) used a similar method, however, assigning a weight to a neighboring pixel based on its distance to the central pixel. Another type of slope calculation methods is based on a polynomial surface. Evans (1980) fitted a six-parameter quadratic equation using a linear regression model, whereas Zevenbergen and Thorne (1987) used a nine-parameter partial quartic equation to model the surface. Slopes are obtained from the analytical derivatives of the surface. Jones (1998) made a rather comprehensive study on the performance of slope estimators and concluded that the finite difference is the best among the eight evaluated methods, whereas D8 seems to give more realistic results at break lines. In our study, the slope calculation is based on the D8 and finite difference methods due to their popularity, simplicity, and mutual complementary properties, which allow us to make certain modification.

Slope by D8 method (S_{D8}) and slope by finite difference method (S_{FD}) are calculated respectively by Equations 1 and 2, where z_i is the elevation at the cell i (see Figure 3), x and y are horizontal coordinates of the DTM, and h is the DTM cell size:

$$S_{D8} = \max_{i=1,8} \frac{z_c - z_i}{\beta h}, \text{ where } \beta = \begin{cases} 1 \text{ when cardinal} \\ \sqrt{2} \text{ when diagonal} \end{cases} \quad (1)$$

$$S_{FD} = \sqrt{\left(\frac{\partial z}{\partial x}\right)^2 + \left(\frac{\partial z}{\partial y}\right)^2} = \sqrt{\left(\frac{z_2 - z_6}{2h}\right)^2 + \left(\frac{z_8 - z_4}{2h}\right)^2}. \quad (2)$$

According to some previous studies (Wilson and Gallant, 2000), the direction in which the elevation difference is calculated by the D8 method may not necessarily be at the steepest descent. Moreover, the location of the estimated slope by the D8 method is assigned to the neighborhood center rather than to the geometric center of the two involved cells as

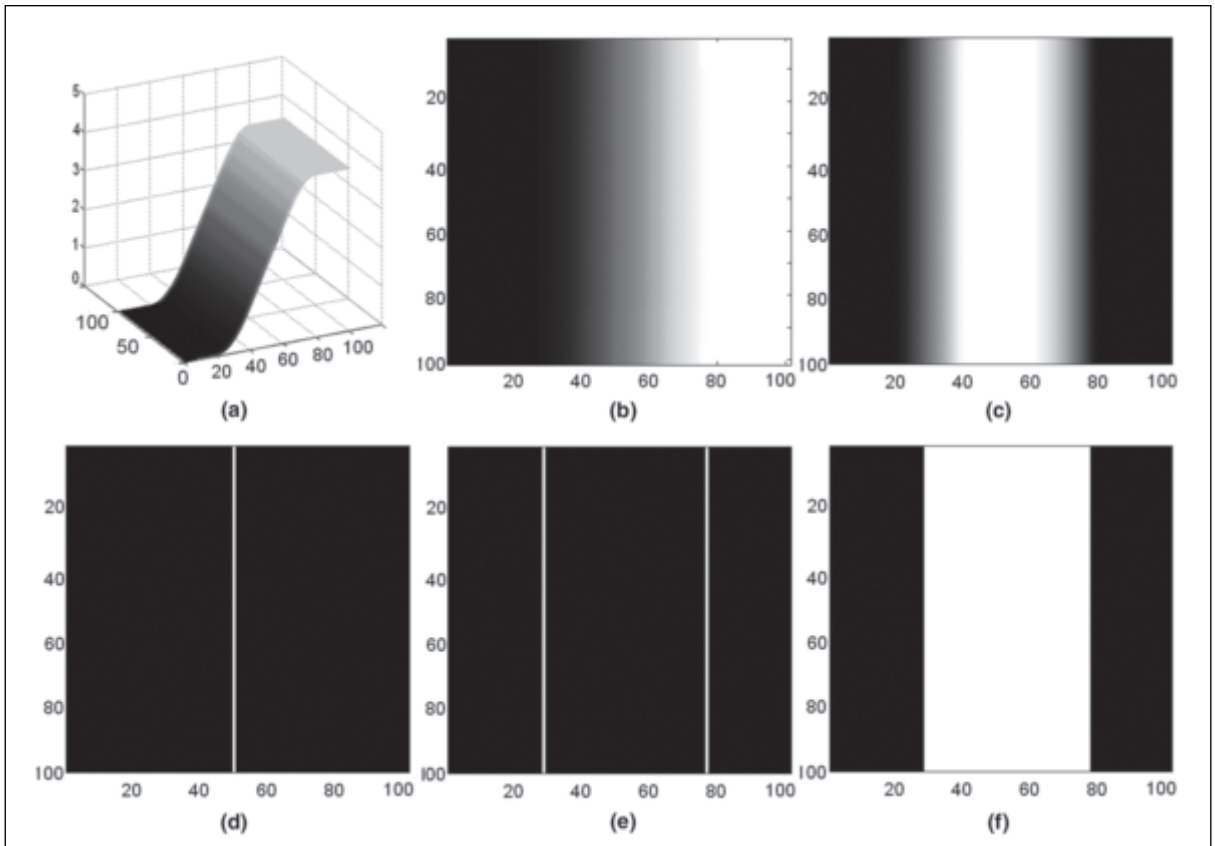

Figure 2. Edge detection: (a) hyperbolic slope surface, (b) DTM, (c) slope map, (d) LOG of DTM, (e) LOG of slope map, and (f) feature with simple edge (white).

it should be. This causes a shift of the detected edge boundary from its correct location. On the contrary, the most reliable slopes can be obtained from the finite difference method (Wilson and Gallant, 2000). Analytically, the smoothness of the finite difference method is due to its larger horizontal distance being possibly two times the one in the D8 method. To demonstrate the above evaluation, the two slope estimators are applied to a DTM of Antarctica containing significant break lines and the results are shown in Figure 4. It is seen that the break lines on the slope map by D8 are wider and more significant than the one from the finite difference.

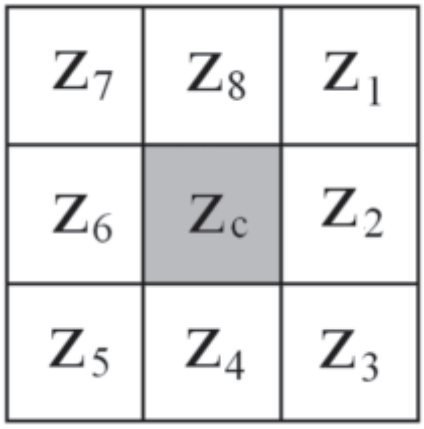

Figure 3. A 3 × 3 DTM neighborhood.

Based on the above analysis, an ideal slope estimator should be able to compensate the shortcomings of the above two methods and keep their good properties. Therefore, we introduce a weighted average of the two methods, i.e.,:

$$S = wS_{D8} + (1 - w)S_{FD} \tag{3}$$

where the weight factor w is chosen as:

$$w = \frac{1}{2}\frac{\left(\sqrt{\left(\frac{\partial z}{\partial x_d}\right)^2 + \left(\frac{\partial z}{\partial y_d}\right)^2} - \sqrt{\left(\frac{\partial z}{\partial x_c}\right)^2 + \left(\frac{\partial z}{\partial y_c}\right)^2}\right)^2}{\left(\left(\frac{\partial z}{\partial x_d}\right)^2 + \left(\frac{\partial z}{\partial y_d}\right)^2 + \left(\frac{\partial z}{\partial x_c}\right)^2 + \left(\frac{\partial z}{\partial y_c}\right)^2\right)} \tag{4}$$

and the partials are calculated by:

$$\frac{\partial z}{\partial x_c} = \frac{z_2 - z_6}{2h}, \quad \frac{\partial z}{\partial y_c} = \frac{z_8 - z_4}{2h}, \quad \frac{\partial z}{\partial x_d} = \frac{z_1 - z_5}{2\sqrt{2}\,h}, \quad \frac{\partial z}{\partial y_d} = \frac{z_7 - z_3}{2\sqrt{2}\,h}. \tag{5}$$

The subscripts c and d are for the cardinal and diagonal directions, respectively. In this way, the modified slope is within the range of the finite difference (min) and the D8 (max). It can be shown that $w_{\max} = 1/2$ and $w \le (1 - w)$, i.e., the weighting strategy is in favor of the finite difference method other than the D8 method. For isotropic topography the slopes in the diagonal and cardinal directions are equal, i.e., $\sqrt{(\partial z/\partial x_d)^2 + (\partial z/\partial y_d)^2} = \sqrt{(\partial z/\partial x_c)^2 + (\partial z/\partial y_c)^2}$; thus, $w = 0$

and $S = S_{FD}$, which means that the finite difference method takes effect. Similarly, for anisotropic topography, the difference between the cardinal slope $\sqrt{(\partial z/\partial x_c)^2 + (\partial z/\partial y_c)^2}$ and the diagonal slope $\sqrt{(\partial z/\partial x_d)^2 + (\partial z/\partial y_d)^2}$ makes the D8 slope contribute to the final slope. As the result of this, the slope of Equation 3 simultaneously amplifies the finite difference and restrains the D8 outcomes. As shown in Figure 4, the slope map from the weighted average slope estimator has more details than the finite difference method and is smoother or less noisy than the D8 method.

Boundary Determination

As addressed above, feature boundary can be defined as a contour of constant slope. The key to determining the boundary is then to determine such critical slope value or threshold. For this purpose, our feature model requires that the feature boundary passes as many edge pixels as possible that have local maximum curvatures (Wang and Bai, 2003). The well-known LOG operator is applied to the slope map to determine edges. The LOG operator is composed of a Gaussian filter for smoothing and a Laplacian filter for the second-order derivative. The Gaussian filter is primarily used to smooth the slope map because the subsequent high-order derivative operation tends to cause noise manifestation (Florinsky, 2002). With proper thresholding, the zero-crossing of LOG will yield the edge pixels. Unlike the previous work that needs prior-knowledge in the binary decision algorithm (Gomes-Pereira and Wicherson, 1999) and in the hysteresis algorithm (Sui, 2002), we intend to automate this process by taking into account the edge connectivity.

The feature boundary should be both connected and rigid to the effect of thresholding. Hence, only pixels that have both significantly small LOG returns and significantly large connectivity will be selected as edge pixels. To automatically determine these significant values, we produce a series of edge images through changing the LOG threshold. The connectivity C for each edge image is calculated with the following formula in a way similar to the maximum sub-boundary length in the sub-boundary statistics (Oden *et al.*, 1993):

$$C = \frac{n}{N} \tag{6}$$

where n is the number of edge pixels with at least two neighbors in the 3×3 neighborhood, and N is the total number of pixels in the edge image. Figure 5 presents some of the edge images produced under different LOG thresholds T_{LoG}, while Figure 6 illustrates the relationship between the LOG threshold T_{LoG} and the connectivity C for these edge images. The LOG threshold that generates the maximum connectivity will then be selected to produce

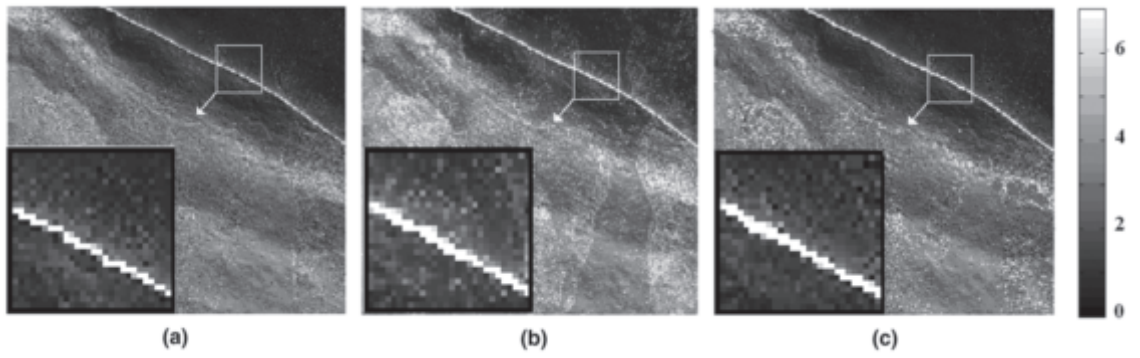

Figure 4. Slopes calculated with different methods: (a) finite difference, (b) D8, and (c) weighted average.

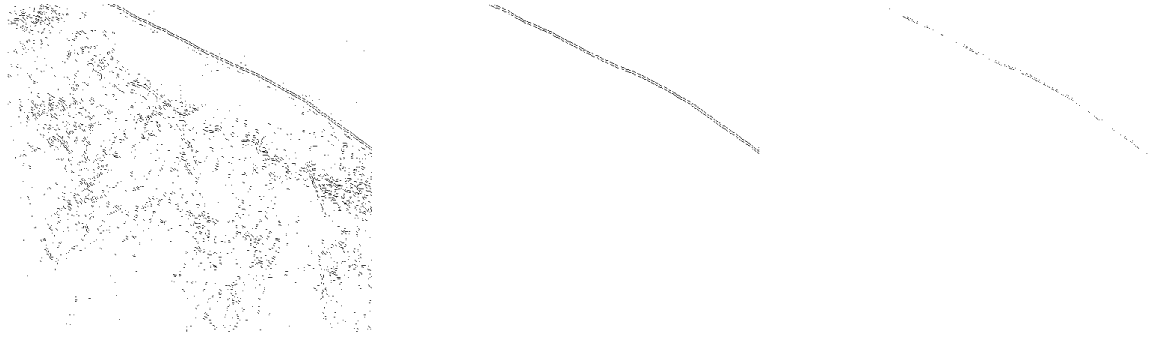

Figure 5. Edge images obtained under different LOG thresholds T_{LoG}: (a) $T_{LoG} = 0.005$, (b) $T_{LoG} = 0.01$, and (c) $T_{LoG} = 0.02$.

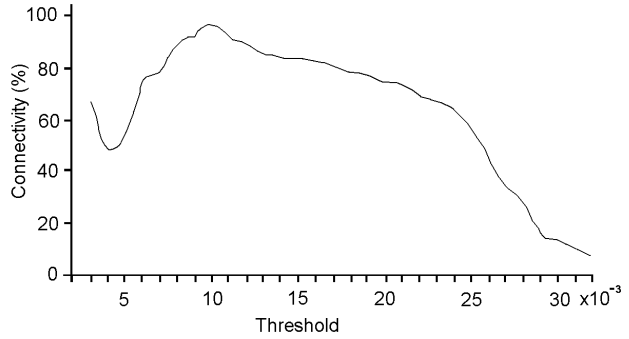

Figure 6. LOG threshold versus connectivity of edges.

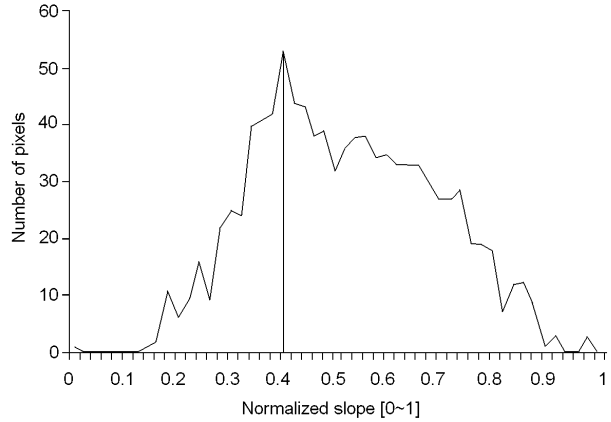

Figure 7. Slope threshold selection on the slope histogram over the edge image.

the final edge image. In this example, the final determined LOG threshold is $T_{LoG} = 0.01$, which leads to a connectivity of 94 percent.

Once the final edge image is obtained, the next step is to determine the slope threshold or the slope contour value for the feature boundary. To consider the location offset (Wang and Bai, 2003) of the edges detected by the LOG operator, the slope of an edge pixel is taken as the average of its two neighboring edge pixels. Finally, the slope histogram over the edge image is used to determine the slope threshold statistically. The slope that yields the largest number of edge pixels is chosen as the slope threshold. In Figure 7, the slopes are normalized from 0 to 1 and the chosen normalized slope threshold is 0.4.

Boundary Tracing

Upon the successful determination of the slope threshold for the feature boundary, the interest topographic feature can be traced. For this purpose, we adopt and modify the marching square algorithm (Lorensen and Cline, 1987). Technically, a bilinear interpolation should be assumed within each DTM cell. However, due to the heavy computing cost for rendering a hyperbola contour, a straight line segment is used instead in the marching square algorithm, whose main idea is outlined below and illustrated in Figure 8. First, pixels in a grid data set are classified into two types, true (inside feature) or false (outside feature), depending on if the cell value (such as slope in this study) is above or below the threshold. In Figure 8, the dark and light dots are for the true and false pixels, respectively, connecting the four adjacent pixels forms a square. The gray area within a square represents the feature interior, while the straight line defines the feature boundary. Since each pixel in a square only has two states (true or false), there are in total $2^4 = 16$ possible configurations for each square. Considering the duplication under rotation, there are only six distinct cases as shown in Figure 8. The original marching square method determines the contour location with a linear interpolation along the edges of the square. As an example, the location of point P off from point A along the edge AB (see Figure 9) is determined by (assume the cell size is one unit):

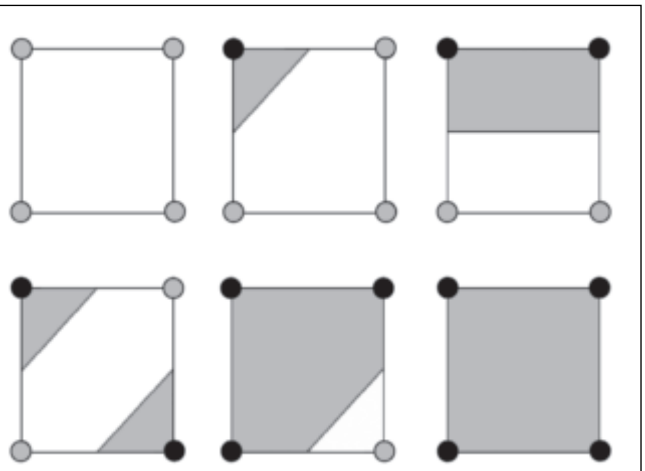

Figure 8. Distinct cases for marching square algorithm (dark dot: inside feature cell; light dot: outside feature cell; shaded area: feature interior).

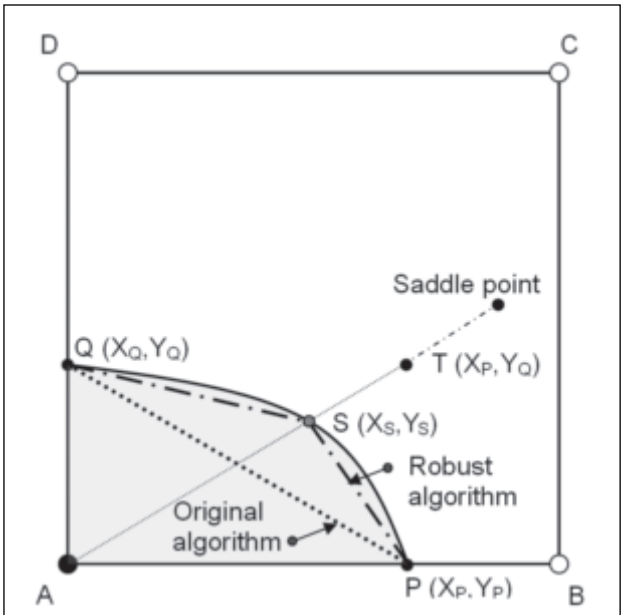

Figure 9. Original and robust marching square methods.

$$X_P = \frac{S_T - S_A}{S_B - S_A};\ Y_P = 0$$
$$X_Q = 0;\ Y_Q = \frac{S_T - S_A}{S_C - S_A} \quad (7)$$

where S_A and S_B are slopes at A and B, and S_T is the slope threshold determined from the previous step. Similarly, the location of Q can be determined by a linear interpolation along the edge AD. The straight line PQ is used as the contour line in the original marching square method. It should be noted that the straight line PQ is an approximation to the hyperbola determined by the bilinear interpolation using the four pixel values. Therefore, the curvature of the contour line is ignored in the original matching square method, which may not sufficiently reflect complex topography.

The improvement to the original marching square algorithm leads to the so-called robust marching square algorithm proposed by Lopes and Brodlie (1998 and 2003). It is developed to extract more accurate iso-surface (contour) and to resolve the ambiguity in the original marching cube algorithm pointed out by Nielson and Hamann (1991). As shown in Figure 9, the robust algorithm adds one point S, which is on the hyperbola and at the maximum distance from the straight line PQ. The newly added point S is called shoulder point, which reduces the gap between the original straight line and the hyperbola. The straight line PQ will then be replaced by the two straight line segments PS and SQ. Although adding the shoulder point can yield a better fidelity to represent the hyperbola contour, we argue that it is not always needed since not every hyperbola will have sufficient curvature to make a significant difference from a straight line.

Based on the above analysis, this study proposes an adaptive marching square algorithm to optimize the number of shoulder points needed to represent a contour. The selection of the shoulder point is based on the difference between the original marching square algorithm and the hyperbola. Several steps are involved in determining and selecting a shoulder point. The first step is to determine the two intersections P and Q of the hyperbola with the two sides of the marching square. Their coordinates can be calculated using the linear interpolation listed in Equation 7. The second step is to determine the shoulder point S in the robust approach. According to (Lopes and Brodlie, 1998), the location of S can be determined by

$$X_S = \frac{\sqrt{(a + be + cf)^2 + 4ce(bf + d)}}{2ce}$$
$$Y_S = eX_S + f \quad (8)$$

where:

$$a = S_B - S_A$$
$$b = S_D - S_A$$
$$c = S_A - S_B + S_C - S_D$$
$$d = S_A - S_T \quad (9)$$
$$e = \frac{Y_P - Y_Q}{X_Q - X_P}$$
$$f = \frac{X_Q Y_Q - X_P Y_P}{X_Q - X_P}$$

The third step is local generalization, i.e., deciding if the shoulder point should be kept for the contour. This will be evaluated by the area of the discrepancy triangle PQS or equivalently the curvature of the hyperbola shown in Figure 9. Only when it is significantly large is necessary adding a shoulder point. In this way, we can reduce the number of shoulder points for contouring while retaining the required resolution. Shoulder points with a discrepancy triangle larger than a given threshold T_Δ will be used in the adaptive approach, while the others will be discarded. Because of this selective capability, the proposed approach is able to optimize the data size for contour representation at a desired fidelity.

Tests and Evaluation

Test Overview

Tests are designed to examine the capabilities and performance of the proposed adaptive feature extraction approach. Three DTM data sets: Arena Valley, Cape Royds, and Mountain Erebus in Antarctica were used for the tests. The data were collected by airborne lidar, processed and delivered by the U.S. Geological Survey (USGS) as a raster DTM at a resolution of 2-meters. The down-sampled 4- and 8-meter DTM is used in this study, while the original 2-meter DTM is used for evaluation purpose only. The DTM data sets are shown in Figure 10 and their properties are listed in Table 1.

The test results are shown in Table 1 and Figure 11. As described above, the LOG operator is applied to the slope map to detect edge pixels while taking into account their connectivity. The final slope threshold is determined by using the histogram of slopes over the edge pixels. Table 1 also lists the LOG threshold values, the edge connectivity, and the slope thresholds for contouring. Shoulder points

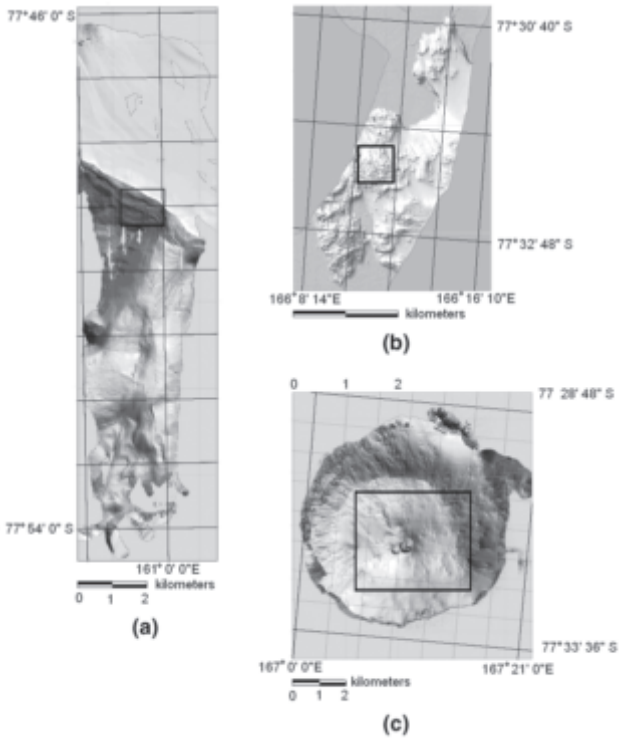

Figure 10. Shaded relief images of Arena Valley (a), Cape Royds (b), and (c) Mt. Erebus areas in Antarctica. The rectangles show the subsets used in this study. The maps were from **http://imsdemo.cr.usgs.gov/website/antarctica/**

TABLE 1. PROPERTIES OF THE ANTARCTIC DTM DATA SETS AND TEST RESULTS

		Arena Valley	Cape Royd	Mt. Erebus
Full resolution	Cell size (m)	2 × 2	2 × 2	2 × 2
	Dimension	2021 × 8001	2001 × 3501	4501 × 5001
Subset used	Cell size (m)	4 × 4	8 × 8	8 × 8
	Dimension	601 × 681	185 × 162	780 × 774
	LOG threshold	0.010	0.002	0.040
Boundary determination	Connectivity(%)	99.4	95.9	87.7
	Slope threshold (normalized)	0.404	0.360	0.625
Original method	Distance error (pixel)	0.58	0.64	0.89
Robust method	# shoulder points	141	602	229
	Distance error (pixel)	0.28	0.52	0.37
Adaptive method (T_Δ = 0.025)	# shoulder points	35	151	58
	Distance error (pixel)	0.37	0.53	0.53

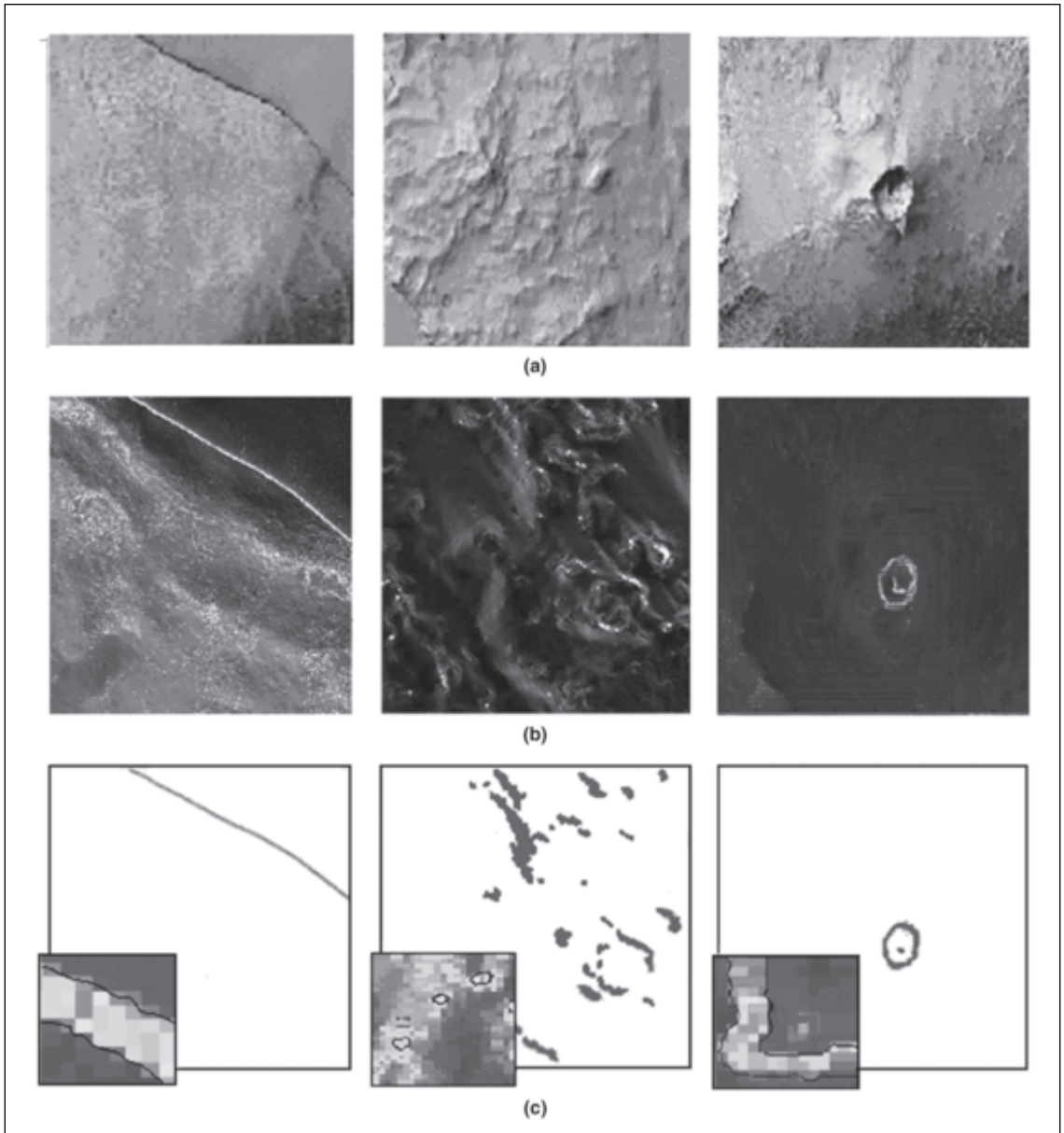

Figure 11. (a) shaded relief images, (b) slope maps (brighter pixels for higher slope), and (c) extracted features.

with discrepancy triangle larger than $T_\Delta = 0.025$ (given the area of one pixel is unit) are selected in the adaptive marching square approach. The distance errors (see next section for details) of the original, robust, and adaptive methods are also listed in Table 1. Shown on the top row of Figure 11 are the shaded relief images of the study areas, while the middle row is the slope maps of the test sites calculated with the weighted average slope estimator. The bottom row of Figure 11 presents the extracted topographic features. The feature boundary defined by the slope threshold is shown as lines in the inset maps for clarity, whereas the grayed areas in the main maps are the feature interior where the slopes are above the slope threshold.

Extracted Features

The selected three DTM data sets contain a variety of topographic features. According to the definition of the Scientific Committee on Antarctic Research (SCAR), topographic features may take three classes of shapes: linear shape, blob shape, and donut shape (**http://aadc-maps.aad.gov.au/aadc/ftc/**). The features within the same class category have the same morphological structures with different sizes and surface materials and with similar shape and appearance. The linear features include canyon, gorge, ravine, and valley; blob shape features consist of knob, knoll, and peak. Examples of donut shape features are cirque, crater, butte, and plateau. As shown in the top row of Figure 11, the selected test area Arena Valley has a big valley as the linear shape feature. Cape Royds has a number of mounts as the blob shape feature, and Mountain Erebus has a few craters as the donut shape feature. Such a selection of the test areas encompasses all types of feature categories defined by the SCAR.

Evaluation Measure

To evaluate the feature extraction results, the reference is taken as the results from the original marching square algorithm applied to the full-resolution 2-meter DTM. Results from the original, adaptive and robust marching square algorithms applied to the down-sampled lower resolution DTM are compared with respect to the reference. As shown in Figure 12, the evaluation is based on the distance between the extracted boundary and the reference boundary (Perez and Vidal, 1994). For each point in the extracted boundary, its distance to the closest reference boundary is calculated. The average of all such distances over all extracted boundary points calculated by Equation 10 is then used to measure the overall precision:

$$E = \frac{1}{N}\sum_{i=1}^{N} d_i \tag{10}$$

where E is the average distance error, d_i is the distance from an extracted boundary point to the closest reference boundary, and N is the number of points in the extracted boundary.

Performance Evaluation

The precision of the adaptive marching square method varies with the number of selected shoulder points. Figure 13 plots such relation over the three data sets. All tests are carried out at the down-sampled resolutions. The vertical axis is the ratio between the average distance errors from the adaptive (E_a) and original (E_o) methods. The relative data size in the horizontal axis is the number of points in the adaptive algorithm relative to the number of points in the original algorithm. The relative data size 1 corresponds to the original method, which is equivalent to no shoulder point being selected in the adaptive method. The relative data size 2 is the robust method in which all shoulder points are included. This is because the number of shoulder points in the robust approach is the same as the number of points in the original marching square method if the feature boundary is treated as a polygon.

Figure 13 shows that the error decreases with the increasing number of shoulder points in a non-linear way. For areas with relatively simple (small curvature) topography, such as Arena Valley and Mount Erebus sites, the error drops more rapidly than in an area with complicated features (Cape Royd), when more shoulder points are included in the adaptive method. This is because the shoulder points in complicated topography tend to have errors with similar magnitudes. Therefore, including more shoulder points in the adaptive method can only slowly improve its precision. On the other hand, errors of shoulder points in areas with simple topography are unlikely evenly distributed. Including shoulder points in a descending order of their discrepancy triangle size can therefore considerably improve the precision of the original method. To be specific, for Arena Valley and Mount Erebus, Figure 13 shows that their errors drop by 40 percent (from 1 to about 0.6) after 30 percent (relative data size 1.3) of the shoulder points are added to the original method. Adding more shoulder points may further increase

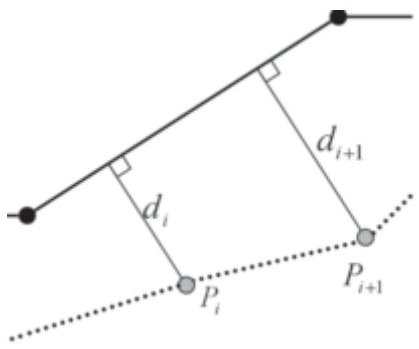

Figure 12. Evaluation measure of the extracted feature. The solid line is the reference boundary and the dot line is the extracted boundary.

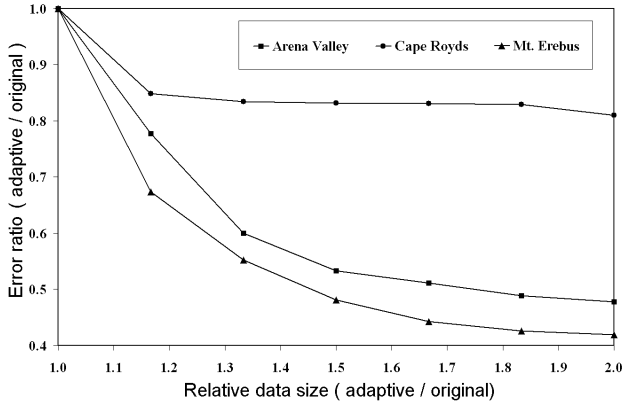

Figure 13. Errors of the extracted features versus the number of shoulder points in the adaptive method.

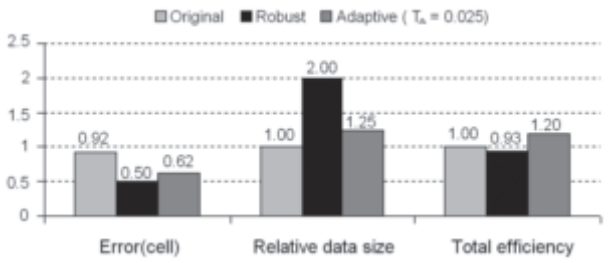

Figure 14. Overall performance of different marching square methods.

the precision, however, at a slower rate. For Cape Royd, adding the first 10 percent shoulder points reduces the error of the extracted features by about ~15 percent, however, the inclusion of additional shoulder points can only slowly improve the precision by several percent.

Similar evaluation can be made with reference to the robust approach in terms of efficient feature representation, storage, and rendering. For complex topography (Cape Royd), reducing up to 80 percent of the shoulder points from the robust approach may only cause a marginal precision loss of less than 10 percent in the adaptive approach. The use of adaptive approach is less advantageous for simple topography. Reducing 50 percent of the shoulder points from the robust approach will cause 20 percent precision loss in the adaptive approach.

The above discussion suggests that the performance of the adaptive algorithm is dependent on the complexity of the topography. Selectively adding shoulder points to the original method can considerably improve the precision for simple topography area, while reducing shoulder points from the robust method is very efficient for complex topography in terms of an optimal balance between precision and resolution.

To gain a general understanding, this section will evaluate the overall performance of the adaptive method for the three data sets. Figure 14 shows the average for all three study areas computed with Equation 10 with relative to the original marching square method. This table is obtained by selecting the shoulder points with a discrepancy area larger than $T_\Delta = 0.025$. The total efficiency in Figure 14 is the overall performance index considering both precision and resolution, and is calculated by:

$$Total\ Efficiency = \frac{E_a}{E_o}\frac{N_a}{N_0} \tag{11}$$

where the E_o and E_a are the errors for the original and adaptive methods, respectively; N_o and N_a are the number of points in the original and adaptive methods. For the original method, this total efficiency index is equal to 1, while for the robust approach the ratio N_a/N_0 is 2. It is seen that the adaptive approach can reduce the error of the original method by 33 percent (0.62 versus 0.92) by using 25 percent of the shoulder points, while its precision is about 24 percent (0.62 versus 0.5) lower than the robust approach. The total efficiency index suggests that the adaptive approach (1.20) is slightly better than the robust (0.93) and original (1.0) ones, both of which have about the same overall balance between precision and resolution.

Conclusions

A new topographic feature extraction approach is proposed and evaluated through this study. Unlike most other studies, we model topographic features as a region with interior and boundary. It is shown that such a model can be used to represent a broad range of topographic features, such as valley, mount, and crater. Determining the slope contour value is the key to localizing the feature boundary. For this objective, the slope contour is required to pass as many connected edge pixels as possible that have local maximum curvatures. As the first step towards the solution, a weighted average of the D8 and finite difference methods is used to produce the slope map. It compensates the weakness of the two existing methods, and the outcome slope map is less noisy than the D8 and more informative than the finite difference. In the second step, a sequence of LOG operations with multiple thresholds are applied to the slope map and result in an satisfactory edge map with maximum connectivity. The slope threshold is then selected such that the slope contour passes as many edge pixels as possible. By considering both the connectivity and the number of edge pixels, this treatment essentially automates the selection of the slope threshold, which is regarded as one of the most difficult tasks in feature extraction. The third step, tracing the feature boundary, is considered as a rendering problem in computer graphics, for which the marching square algorithm and its robust modification are adopted and enhanced with adaptive capability. The proposed adaptive approach can select the necessary shoulder points based on the local topographic complexity such that a balance between resolution and precision can be achieved. It is found that the performance of the adaptive algorithm depends on the topographic complexity. For complex topography, adding additional shoulder points will slowly improve the precision of the original marching square algorithm; which implies the number of shoulder points in the robust marching square algorithm can be considerably reduced without losing much precision. Similar observation is made for simple topography where adding or removing shoulder points may have significant effect on the precision of the extracted features. It is shown overall reducing 75 percent (2.00 versus 1.25) of the shoulder points from the robust approach will cause 24 percent (0.50 versus 0.62) precision drop in the adaptive method.

Despite the above successful initiative and experience, future efforts can be made on several related aspects. First, the performance and capability of the proposed approach can be further investigated comprehensively for more types of topography. Its principles need to be formulated and tested with man-made features such as buildings embedded in a digital surface model. Investigation is needed to look into the properties of the proposed slope estimator and present a quantitative evaluation against other typical slope estimators such as the ones based on surface modeling. Finally, scale or resolution remains to be a fundamental issue in the proposed approach as in many other feature extraction methods. It would be theoretically interesting to associate the scale space theory to the developed slope thresholding method. Moreover, the performance of the proposed feature extraction steps may also be examined for DTM at different resolutions.

Acknowledgment

This work was partially funded by a USGS grant.

References

Argialas, D., and A. Tzotsos, 2006. Automatic extraction of physiographic features and alluvial fans in Nevada, USA, from digital elevation models and satellite imagery through multiresolution segmentation and object-oriented classification, *Proceeding of*

the ASPRS Annual Conference, 01–05 May, Reno, Nevada, unpaginated CD-ROM.

Band, L.E., 1986. Topographic partition of watersheds with digital elevation models, *Water Resources Research*, 22:15–24.

Bowen, Z.H., and R.G. Waltermire, 2002. Evaluation of light detection and ranging (LIDAR) for measuring river corridor topography, *Journal of the American Water Resources Association*, 38(1):33–41.

Briese, C., 2004. Three-dimensional modeling of breaklines from airborne laser scanner data, *International Archives of Photogrammetry and Remote Sensing*, Istanbul, Turkey, Vol. XXXV, B3, pp. 1097–1102.

Brock, J.C., C.W. Wright, A.H. Sallenger, W.B. Krabill, and R.N. Swift, 2001. Recognition of fiducial surfaces in lidar surveys of coastal topography, *Photogrammetric Engineering & Remote Sensing*, 67(11):1245–1258.

Brügelmann, R., 2000. Automatic breakline detection from airborne laser range data, *International Archives of Photogrammetry and Remote Sensing*, Amsterdam, Netherlands, Vol. XXXIII, B3 pp. 109–115.

Brzank, A., P. Lohmann, and C. Heipke, 2005. Automated extraction of pair wise structure lines using airborne laser scanner data in coastal areas, *Proceedings of the ISPRS WG III/3, III/4, V/3 Workshop: Laser Scanning 2005*, Enschede, Netherlands, September 12–14, unpaginated CD-ROM.

Cobby, D.M., D.C. Mason, and I.J. Davenport, 2001. Image processing of airborne scanning laser altimetry data for improved river flood modeling, *ISPRS Journal of Photogrammetry and Remote Sensing*, 56:121–138.

Evans, I., 1980. An integrated system of terrain analysis and slope mapping, *Zeitschrift für Geomorphologie*, N.F. Supplementband, 36, 274–295.

Fleming, M.D., and R.M. Hoffer, 1979. Machine processing of Landsat MSS data and DMA topographic data for forest cover type mapping, *LARS Technical Report 062879*, Laboratory for Applications of Remote Sensing, Purdue University, West Lafayette, Indiana.

Florinsky, I.V., 1998. Precision of local topographic variables derived from digital elevation models, *International Journal of Geographical Information Science*, 12:47–62.

Florinsky, I.V., 2002. Error of signal processing in digital terrain modeling, *International Journal of Geographical Information Science*, 16(5):475–501.

Gomes-Pereira, L., and R. Wicherson, 1999. Suitability of laser data for deriving geographical information - A case study in the context of management of fluvial zones, *ISPRS Journal of Photogrammetry and Remote Sensing* 54:105–114.

Guthrie, V., and E. Simental, 2003. Detecting micro-terrain features using high resolution interferometric synthetic aperture radar (IFSAR), *Proceedings of the ASPRS 2003 Annual Conference*, Anchorage, Alaska, May, unpaginated CD-ROM.

Hooper, D.M., M.I. Bursik, and F.H. Webb, 2003. Application of high-resolution, interferometric DEMs to geomorphic studies of fault scarps, Fish Lake Valley, Nevada-California, *USA, Remote Sensing of Environment*, 84(2):255–267.

Horn, B.K.P., 1981. Hill shading and the reflectance map, *Proceedings of the Institute of Electrical and Electronics Engineers (IEEE)*, 69(1):14–47.

Jenson, S.K., and J.O. Domingue, 1988. Extracting topographic structure from digital elevation data for geographic information system analysis, *Photogrammetric Engineering & Remote Sensing*, 54(11):1593–1600.

Jones, K.H., 1998. A comparison of algorithms used to computer hill slope as a property of the DTM, *Computers & Geosciences*, 24(4):315–323.

Koenderink, J.J., 1990. *Solid Shape*, The MIT Press, Cambridge, Massachusetts.

Lopes, A., and K. Brodlie, 1998. Precision in contour drawing, *Proceedings of the Eurographics UK 98 Conference*.

Lopes, A., and K. Brodlie, 2003. Improving the robustness and precision of the marching cubes algorithm for isosurfacing, *IEEE Transactions on Visualization and Computer Graphics*, 9(1):16–29.

Lorensen, W.E., and H.E. Cline, 1987. Marching cubes: A high resolution 3D surface construction algorithm, *Computer Graphics*, 21:163–169.

Mark, D.M., 1984. Automatic detection of drainage networks from digital elevation models, *Cartographica*, 21:168–178.

Marr, D., and E. Hildreth, 1980. Theory of edge detection, *Proceedings of the Royal Society of London, B.*, 207(1167):187–217.

Miliaresis, G., and D. Argialas, 1999. Segmentation of physiographic features from the global digital model/GTOPO30, *Computers & Geosciences*, 25:715–728.

Moore, I.D., R.B. Grayson, and A.R. Ladson, 1991. Digital terrain modeling: A review of hydrological, geomorphological, and biological applications, *Hydrological Processes*, 5:3–30.

Morris, R., 1996. The sub-parabolic lines of a surface, *Mathematics of Surfaces VI* (G. Mullineux, editor), Clarendon Press, Oxford, pp. 79–102.

Nielson, G.M., and B. Hamann, 1991. The Asymptotic Decider: Resolving the ambiguity in marching cubes, *Proceedings of the Visualiration'91*, IEEE Computer Society Press, pp. 83–90.

O'Callaghan, J.F., and D.M. Mark, 1984. The extraction of drainage network from digital elevation data, *Computer Vision, Graphics and Image Processing*, 28:323–344.

Oden, N.L., R.R. Sokal, M.J. Fortin, and H. Goebl, 1993. Categorical wombling: Detecting regions of significant change in spatially located categorical variables, *Geographical Analysis*, 25:315–336.

Perez, J.C., and E. Vidal, 1994. Optimum polygonal approximation of digitized curves, *Pattern Recognition Letters*, 15:743–750.

Ramsay, J.G., 1967. *Folding and Fracturing of Rocks*, McGraw Hill, New York

Rango, A., K. Havstad, W. Kustas, T. Schmugge, M. Chopping, and J. Ritchie, 2000. Morphological characteristics of shrub coppice dunes in desert grasslands of southern New Mexico derived from scanning LIDAR, *Remote Sensing of Environment*, 74(1):26–44.

Sui, L., 2002. Processing of laser scanner data and automatic extraction of structure lines, *International Archives of Photogrammetry and Remote Sensing*, Xian, P.R. China, Vol. XXXIV, pp. 429–435.

Tarboton, D.G., 1997. A new method for the determination of flow directions and upslope areas in grid digital elevation models, *Water Resource Research*, 33:309–319.

Turcotte, R., J.P. Fortin, A.N. Rousseau, S. Massicotte, and J.P. Villeneuve, 2001. Determination of the drainage structure of a watershed using a digital elevation model and a digital river and lake network, *Journal of Hydrology*, 240(3–4):225–242

Vogt, J., R. Colombo, and F. Bertolo, 2003. Deriving drainage networks and catchment boundaries: A new methodology combining digital elevation data and environmental characteristics, *Geomorphology*, 53(3–4):281–298.

Wang, L., and J. Bai, 2003. Threshold selection by clustering gray levels of boundary, *Pattern Recognition Letters*, 12:1983–1999.

Wilson, J.P., and J.C. Gallant, 2000. Digital terrain analysis. *Terrain analysis: Principles and Applications* (J.P. Wilson and J.C.Gallant, editors), Wiley, New York, pp.1–27.

Woolard, J.W., and J.D. Colby, 2002. Spatial characterization, resolution, and volumetric change of coastal dunes using airborne LIDAR: Cape Hatteras, North Carolina, *Geomorphology*, 48:269–287.

Zevenbergen, L., and C. Thorne, 1987. Quantitative analysis of land surface topology, *Earth Surface Processes and Landforms*, 12:47–56.

(Received 16 August 2007; accepted 09 November 2007; revised 18 January 2008)